PROCEEDINGS OF SCIENCE

Nucleon charges from Lattice QCD and their implications for BSM physics

Rajan Gupta[a,*]

[a] *Los Alamos National Laboratory, Theoretical Division T-2, Los Alamos, NM 87545, USA*

E-mail: rg@lanl.gov

An overview of the lattice QCD calculations of the charges, $g^{u,d,s}_{A,S,T}$, of nucleons and their implications for SM and BSM physics is presented. The axial charges, $g^{u,d,s}_{A}$, give the contribution of the intrinsic spin of the quarks to the nucleon; the tensor charges, $g^{u,d,s}_{T}$, give the contribution of the quark electric dipole moment operator to the nucleon EDM and are also the second Mellin moments of the transversity distribution of quarks in nucleons; and from the scalar charges $g^{u,d,s}_{A}$, we calculate the pion-nucleon sigma term $\sigma_{\pi N}$ and the strangeness content, σ_s, of the nucleon. The lattice QCD results for these charges are, in most cases, the most precise and are being used as input in phenomenological analyses. The complete set of charges, $g^{u,d,s,c,b,t}_{A,P,S,T,V}$, give the couplings, in low energy effective field theory formulation, of dark matter or novel Higgs-like interactions with nucleons in various Lorentz channels.

The XVIth Quark Confinement and the Hadron Spectrum Conference (QCHSC24)
19-24 August, 2024
Cairns Convention Centre, Cairns, Queensland, Australia

*Speaker

PoS(QCHSC24)009

1. Introduction

Neutrons and protons, the bound states of quarks and gluons, make up most of the observed mass of the universe. Neglecting the Θ term in the definition of Quantum Chromodynamics (QCD), all quantities impacted by the strong interactions (dynamics of quarks and gluons) are calculable in terms of the masses of $n_f = 6$ quark flavors and one fundamental scale, or equivalently the coupling $\alpha_s(Q^2)$ as these two are related by dimensional transmutation. Since $\alpha_s(Q^2)$ is scale dependent, with Q^2 a typical momentum flowing in the process, quantitative analyses of QCD fall into (i) the high energy regime probed in accelerators where α_s is small (QCD becomes asymptotically free) and perturbation theory in α_s becomes reliable, and (ii) low energy, ($\lesssim 1$ GeV), where non-perturbative methods are needed since α_s grows to $O(1)$ (confinement). This second regime encompasses almost all terrestrial phenomena. Large scale simulations of Lattice QCD, i.e., QCD formulated in Euclidean time on a discrete space-time lattice, are now providing many properties of hadrons with increasing precision and impacting phenomenology. Results that the community considers robust with respect to control over statistical and systematic errors are now reviewed regularly by the Flavor Lattice Averaging Group (FLAG) [1, 2]. This talk addresses the status of the calculations of the static properties of neutrons and protons, i.e., their charges, and provides the connections to probes of both the standard model (SM) and beyond the standard model (BSM) physics. The discussion will be limited to the three light quark flavors—the up, down and strange quarks—as the heavier quarks do not significantly impact the properties of the hadrons composed of light quarks. Also, only $\{m_l, m_s\}$ will be the 2 tunable quark masses assuming isospin symmetric $m_l = m_u = m_d$ data.

Weak, electromagnetic and BSM interactions give tiny corrections to properties governed by QCD. Furthermore, interactions that violate the symmetries of QCD, for example, charge-conjugation-parity (CP), generate new properties such as electric dipole moments (EDMs) as discussed in Sec. 8.

The fundamental outputs of lattice QCD are the spectrum of hadrons, matrix elements (ME) of various operators composed of quarks and gluons, between the ground state of these hadrons, and the properties of QCD at finite temperature. These operators, in an effective field theory framework, include both fundamental and effective operators encapsulating BSM physics. The simplest observables are the charges of nucleons, $g^{u,d,s}_{A,S,T,V}$, extracted from the matrix elements of axial, scalar, tensor and vector quark bilinear operators, $\overline{q}\Gamma q$ with the Dirac matrix $\Gamma = \gamma_\mu\gamma_5, I, \sigma_{\mu\nu}, \gamma_\mu$, respectively. Of these, axial and vector are part of the SM while scalar and tensor arise from loop effects or explicitly in BSM theories. This talk presents a status report on their calculations and provides the connections between them and the SM and BSM physics they impact. In particular, I will discuss:

- The isovector axial vector charge, g_A^{u-d}, that gives the strength of the weak interactions with nucleons. See the FLAG 2024 report [1] for the status.
- The charges $g_A^{u,d,s}$ that give the contributions of the intrinsic spin of the quarks to the nucleon spin [3]. See Sec. 7.
- The tensor charges, $g_T^{u,d,s}$, that give the contribution of the quark EDMs to the neutron/proton EDM [4]. They are also the first Mellin moments of the transversity distribution of quarks within nucleons measured in semi-inclusive deep inelastic scattering. See Sec. 8.
- The magnetic dipole moment and electromagnetic form factors of nucleons from the ME of the vector current. Unfortunately, the topic of form factors will not be covered here. For a review of

the axial vector isovector form factors, see [5].

- The isovector scalar and tensor charges, $g^{u-d}_{\{S,T\}}$, can arise due to loop effects or novel BSM interactions. These are being extracted both from low-energy experiments, i.e., from high precision analyses of neutron decay, and at the LHC. For background see Refs. [6, 7], and Ref. [2] for the latest results and details.
- The pion-nucleon sigma term, $\sigma_{\pi N} = m_{u,d} \times g^{u+d}_S$, that gives the nucleon mass generated by the quark mass in the small quark mass approximation [8], and the strangeness content of nucleons, given by $\sigma_s = m_s g^s_S$. These quantities are discussed in Sec. 9
- The full set of charges, $g^{u,d,s}_{A,P,S,T,V}$, also give the strengths of the lowest order interactions, in various Lorentz channels, of dark matter and their mediators or of novel Higgs-like interactions with nucleons as discussed in Sec. 6.

Nucleon charges are extracted from the forward ME, i.e., with zero momentum insertion, of the flavor diagonal quark bilinear operators, $O^q_\Gamma(x) = \bar{q}(x)\Gamma q(x)$ with $q \in \{u, d, s\}$, using the relation

$$\langle n(s_f, \mathbf{p}=0)|Z_\Gamma \bar{q}\Gamma q|n(s_i, \mathbf{p}=0)\rangle = Z_\Gamma g^{q,\text{bare}}_\Gamma \bar{u}(s_f)\Gamma u(s_i)\,, \tag{1}$$

with $u(s)$ the nucleon spinor and Z_Γ the renormalization factor. The ME are obtained from 3-point correlation functions whose quark-line diagrams are shown in Fig. 1.

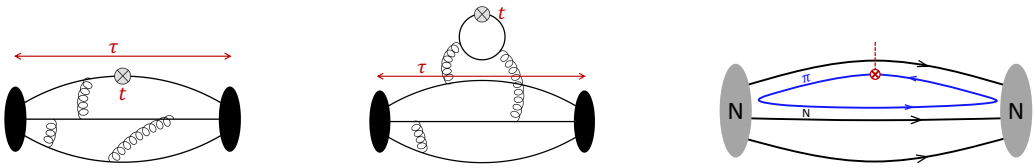

Figure 1: The connected (left) and disconnected (middle) quark-line diagrams that contribute to the 3-point functions from which the matrix element of flavor-diagonal operators are extracted. The black and gray blobs denote the nucleon source and sink separated by Euclidean time τ. The operator, shown by the symbol $\otimes$, is inserted at all intermediate times t between the nucleon source and sink points. The right diagram, redraw of the middle, illustrates the $N\pi$-intermediate state that can give an enhanced contribution for the scalar operator.

To get non-perturbative values of these ME, we need to know the nucleon state in the fully quantum QCD vacuum. Lattice QCD provides both the QCD vacuum and the Euclidean time evolution of hadron states in it, *albeit* in a computer as an ensemble average over a statistical sample of gauge configurations representing the path integral. Briefly, the steps in the calculation are:

- After Wick rotation to Euclidean time ($t \to it$ and $e^{iS} \to e^{-S}$), QCD, discretized on a space-time lattice, can be simulated as a 4-dimensional classical statistical mechanics system using the Feynman path integral formulation. Correlation functions are then calculated as ensemble averages over importance sampled gauge field configurations generated with the Boltzmann weight, e^{-S}.
- The fermions in the path integral are integrated out exactly leaving the QCD action $S = S_{gauge} + \sum_{n_f} \log(\text{Det } M[U]_f)$, a functional of only the gauge fields U. Here the sum in the second term is over the determinant of the Dirac matrix M_f for each of the n_f quark flavors. This non-local determinant retains fermions properties such as the Pauli principle.
- These configurations provide a statistical representation of the QCD vacuum.

- To construct the quark-line diagrams illustrated in Fig. 1, the fully non-perturbative Feynman propagator, $P^{i\to j}_{a\to b}(x \to y)$, is calculated by inverting the Dirac matrix M. It gives the propagation of a quark with spin i and color a from space-time point x to point y, spin j and color b. One column (or row) of M^{-1} is the solution for all end points y on the lattice. A very efficient multigrid method [9] is used for this inversion, nevertheless its calculation consumes a large fraction of the total computer time.
- Correlation functions are then calculated by stitching together these quark propagators with the operators—both interpolating operators for creating/annihilating the states and operator used as probes of the physics and inserted at intermediate times t.
- The evolution in Euclidean time is given by the transfer matrix $\mathcal{T} = e^{-\mathcal{H}t}$. Thus, the propagation of excited states are exponentially suppressed, and for appropriately large t and $\tau - t$, the ground-state is isolated. ME calculated with large t and $\tau - t$ are considered as within ground-state hadrons.
- Energies of the states and ME at single time t within these states are extracted by making fits to the spectral decomposition of respective correlation functions. Both of these quantities are the same in Euclidean and Minkowski time, so no rotation of lattice values back to Minkowski time is required. See Sec. 2.
- Each simulation provides quantities at a given value of the lattice spacing a, lattice size L, and quark masses m_l and m_s, i.e., these data points are defined by $\{a, L, M_\pi, M_K\}$.
- The bare lattice quantities are renormalized and connected to a continuum scheme such as $\overline{\text{MS}}$ at scale 2 GeV used by phenomenologists when analyzing experimental results. These renormalization factors for quark bilinears, Z, are calculated nonperturbatively on the lattice in, for example, the regularization independent symmetric momentum subtraction (RI-sMOM) scheme [10, 11]. These Zs are then matched to the $\overline{MS}$ scheme and run to 2 GeV using perturbation theory. Systematics due to uncertainty in Zs have been controlled to within 1–2%.
- Calculations are done at many $\{a, m_i, L\}$. Physical results are then obtained by extrapolation of the renormalized data collected at these $\{a, m_i, L\}$ to $\{a \to 0, m_i \to m_i^{\text{physical}}, L \to \infty\}$ using physically motivated fit ansatz.

Discretization of QCD on a Euclidean space-time lattice introduces systematic uncertainties and the numerical evaluation of the path integral (ensemble average over gauge configurations) introduces statistical errors. The major sources of errors in the calculations of the nucleon charges are:

- Statistical: The signal-to-noise (S2N) ratio in all nucleon correlation functions falls exponentially as $e^{-(M_N - 1.5M_\pi)t}$ [12, 13]. At present, the signal in the highest statistics calculations extends to $\approx$ 2 fm in 2-point functions, to $\approx$ 1.5 fm in 3-point functions, ... No method exists yet to fundamentally ameliorate this S2N problem.
- At these distances, the excited states contributions (ESC) are significant. These artifacts have to be removed to get ground state matrix elements (GSME). The solution to removing these ESC is to fit the correlation functions to their spectral decomposition keeping as many excited states as allowed by the statistical precision. This is discussion in Sec. 2. Current statistics allow fits keeping up to 1–2 excited states. Resolving and removing the contributions of excited states to nucleon correlation function continues to be a leading systematic. .
- The extrapolation to $\{a \to 0, m_i \to m_i^{\text{physical}}, L \to \infty\}$ requires sufficient number and range of data points in all three variables $\{a, m_i, L\}$. In short, to enable keeping all the significant terms

in the physically motivated ansatz. See Sec. 5.

- Our recent lattice QCD analyses of the nucleon axial vector form factor $G_A(Q^2)$ [5, 14–16] and of the pion-nucleon sigma term $\sigma_{\pi N}$ [8] presented evidence of larger-than-expected excited-state contributions (ESC) from $N\pi$ and $N\pi\pi$ multihadron excited states to the nucleon 3-point correlation functions. Motivated by these works, we continue to study the impact of including $N\pi/N\pi\pi$ states in the analysis of all the flavor diagonal nucleon matrix elements. See Sec. 3.
- To choose between fit strategies—"standard" using first excited-state mass from the 2-point function versus that of the $N\pi$ state—for the final results, we incorporate input from χPT and physics since often the χ^2 of the fits, by themselves, do not resolve between the two.

2. Correlation functions and their Spectral Decomposition

For a unitary formulation of lattice QCD, the spectral decomposition of all 2-point functions is

$$C^{\rm 2pt}(\tau) \equiv \langle \mathcal{N}(\tau)\mathcal{N}(0) = \sum_{i=0}^{3} |\mathcal{A}_i|^2 e^{-M_i\tau} \,. \tag{2}$$

Fits to lattice data for $C^{\rm 2pt}(\tau)$ give, in principle, the amplitudes for creation/annihilation of the states, $\mathcal{A}_i$, and the masses, M_i (energies for nonzero-momentum correlators), of all states that couple to the nucleon interpolating operator $\mathcal{N}$. The challenge is these fits are not well-constrained—large regions of parameter space give similar χ^2 for even 3-state fits. Furthermore, extracting/identifying states that have tiny $\mathcal{A}_i$ but may contribute significantly to higher n-point functions is challenging.

The GSME $\langle 0|O^q_\Gamma|0\rangle$, and from them $g^{q;\rm bare}_\Gamma$ using Eq. (1), are extracted from fits to the spectral decomposition of the spin-projected 3-point functions $C^{\rm 3pt}_\Gamma(t;\tau)$:

$$C^{\rm 3pt}_\Gamma(t;\tau) \equiv \langle \mathcal{N}(\tau)O^q_\Gamma(t)\mathcal{N}(0) = \sum_{i,j=0} \mathcal{A}_i^*\mathcal{A}_j\langle i|O^q_\Gamma|j\rangle e^{-M_i t - M_j(t-\tau)} \tag{3}$$

where $O^q_\Gamma(t)$ is the operator, i.e., the probe, inserted at time t. While the ESC decrease exponentially with source-sink separation τ, the signal-to-noise ratio in the $C^{\rm 3pt}_\Gamma$ also degrades exponentially as $e^{-(M_N - 3/2M_\pi)\tau}$ [12, 13]. Consequently, even 2-state fits to Eq. (1) with all $\mathcal{A}_0$, M_i and the $A_i^*A_j\langle i|O^q_\Gamma|j\rangle$ left as free parameters are poorly constrained. With current data, the $C^{\rm 3pt}_\Gamma$ are well-measured only up to source-sink separation $\tau \approx 1.5$ fm, and for $\tau \lesssim 1.5$ fm ESC are found to be significant as illustrated in Fig. 3. The analysis becomes much more stable if one can input, as priors, the key quantities, $\mathcal{A}_0$ and M_i, from fits to other correlation functions or from phenomenology.

3. Removing excited-state contributions in nucleon correlation functions

Most readers interested in phenomenology can skip this section as it describes a lattice detail. On the other hand, controlling and removing excited-state contributions is key to obtaining high precision results for nucleon calculations and is a good illustration of lattice QCD exhibiting all the expected subtleties of field theory. Solving this problem is a challenge to the younger practitioners!

The interpolating operator $\mathcal{N}$ couples to multihadron $(N(\vec{p}=1)\pi(\vec{p}=-1), N(0)\pi(0)\pi(0), \ldots)$, and radial $(N(1440), \ldots)$ excited states, i.e., all states with $(1/2^+)$ nucleon quantum numbers. The

former are towers of states that become arbitrarily dense as $\vec{p} \to 0$. Note that the contributions of roughly degenerate set of states to Eq. (3) can be treated as one term: the effective amplitude equaling the sum of the amplitudes, which is never used after the fit, i.e., only their common energy M_i is relevant. For example, the $N(\vec{p}=1)\pi(\vec{p}=-1)$ and $N(0)\pi(0)\pi(0)$ are approximately degenerate, so I use the label "$N\pi$" to imply their joint contribution. One can recast Eq. (3) in terms of groups of nearly degenerate states that give significant ESC and focus on determining an M_i for them.

In general, the coupling of a "local" $\mathcal{N}$ to a multihadron state is suppressed by the normalizing factor $1/L^3$ for each additional particle created. Consequently, one would presume that the contribution of multihadron "$N\pi$" states to n-point functions should be tiny. In reality, we know examples where "$N\pi$" contributions to certain matrix elements (thus to the corresponding 3-point functions) are sufficiently enhanced to compensate for the $1/L^3$ suppression of the creation/annihilation amplitude [8, 14]. Two examples suggested by χPT are: (i) the pseudoscalar, G_P, and induced pseudoscalar, $\widetilde{G}_P$, form factors (FF) extracted from the pseudoscalar/axial current [17] and (ii) the scalar charges $g_S^{u,d}$ [8]. The quark line diagrams illustrating this enhancement are shown in Fig. 2 (left and middle). These are in addition to the standard 1-loop χPT contribution shown in Fig. 2 (right) that is applicable to all charges. In the case of the extraction of the axial FF, the analysis (χ^2) of the fit to the lattice data for the A_4 correlator confirmed the enhanced contribution and the need for including the $N\pi$ state in the fit. The resulting FF validate this need as they satisfy the PCAC relation to within expected discretization effects, i.e., the deviations decreased from a factor of ≈ 2 to about 10% [14, 16]. Such a data driven confirmation has not yet been achieved for $g_S^{u,d}$!

A data-driven method would be established if the χ^2 of the fits in the following two analyses differed. (i) using $M_1 \approx 1250$ MeV ($N\pi$ case) and (ii) $M_1 \approx 1500$ MeV (standard case with M_1 close to the radial excitation $N(1440)$ mass and assuming multihadron states can be neglected). In practice, the number of states that can be kept in the spectral decomposition is dictated by the statistical quality of the data, and, unfortunately, the χ^2 of current fits do not, *a priori*, distinguish between the "standard" versus "$N\pi$" analyses even though the M_1 are quite different. The $\tau \to \infty$ values with these two M_1 are, however, significantly different. As a result, fits to current data with even 2 excited states use external inputs, notably of the mass gap ($\Delta M_1 = M_1 - M_0$), rather than predicting them.

There are 4 approaches being explored: (i) Take the ground state amplitude A_0 and masses M_i from fits to the nucleon 2-point correlation functions constructed using the same interpolating operator $\mathcal{N}$. The shortcoming is—these fits do not expose the $N\pi$ states due to the $1/L^3$ suppression. (ii) Take the M_i from some other related 3-point functions with enhanced ME. This strategy works for the axial FF analysis [17]. (iii) Input the phenomenological values of excited states motivated by χPT via narrow priors. This is used for $g_S^{u,d}$ in [8] and the axial FF in [18]. (iv) Construct a variational ansatz for the $\mathcal{N}$ and carry out a generalized eigenvalue analysis [19]. This strategy will be challenging if a number of multihadron states are needed. Compounding the issue of developing data-driven methods, note that the $M_{N(1)\pi(-1)}$ becomes smaller than M_{radial} only for $M_\pi \lesssim 200$ MeV. Thus, to even expose/quantify these effects, one needs data from multiple ensembles generated with $M_\pi \lesssim 200$ MeV.

We are currently investigating strategy (i), i.e., use much higher statistics data on two physical masses ensembles to push the analysis to values of τ at which the 3-state fits to (i) the "standard" approach with M_1 and M_2 taken from a simultaneous fit to 2-point function within a jackknife/bootstrap

procedure, and (ii) the "$N\pi$" approach with $M_1 = M_{N\pi}$, the energy of the non-interacting state using lattice energies and input using narrow priors, and M_2 the first excited state mass in the 2-point fit are distinguished by the χ^2. This would constitute a data-driven resolution for observables needing the $N\pi$ state to be included in the ESC analysis.

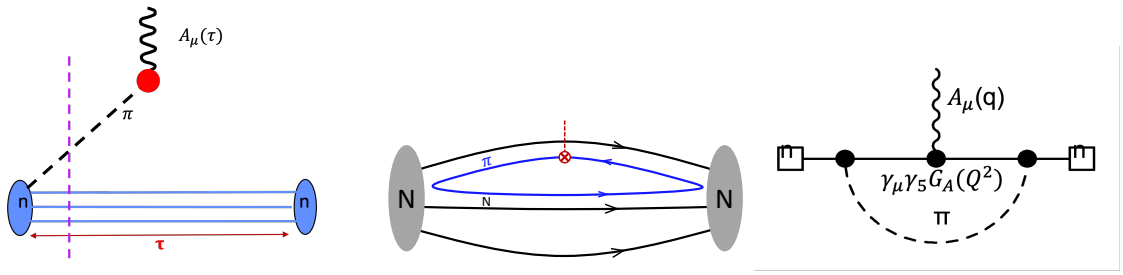

Figure 2: Quark line diagrams illustrating the contribution of $N\pi$ states. (Left) The current A_μ annihilates the pion in the $N\pi$ state produced by the nucleon source. Since the pion is light, the A_μ can couple to it anywhere on the time slice , i.e., giving a compensating enhancement of L^3. See Ref. [5] for a review. (Middle—relevant to $g_S^{u,d}$) the scalar current couples to a light quark loop creating an enhanced $N\pi$ state [8]. (Right) The standard pion loop contribution to all charges that could be $O(5\%)$ be as suggested by χPT.

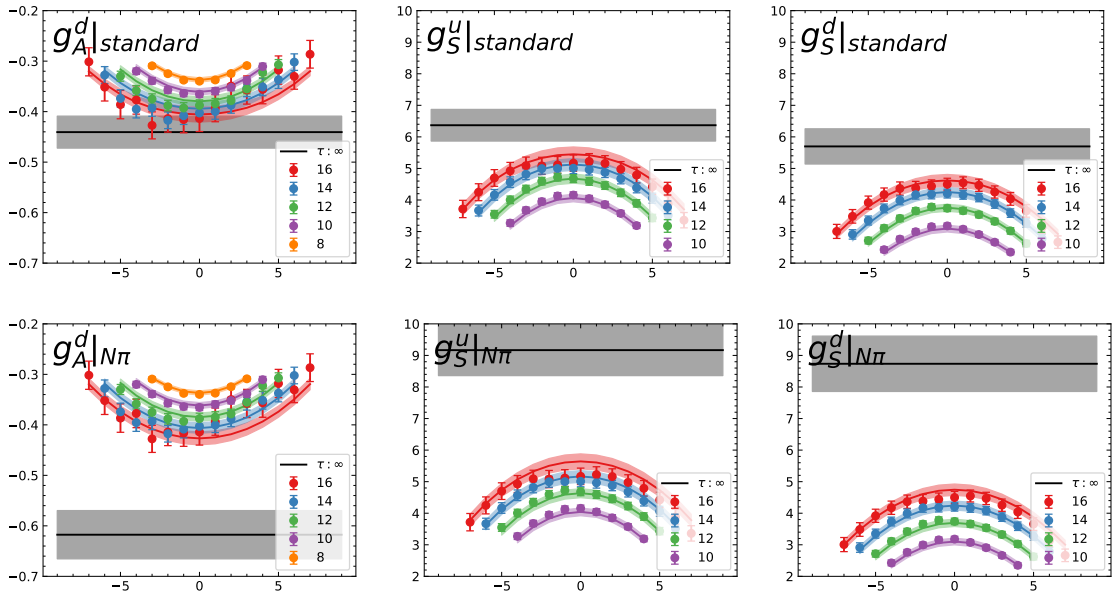

Figure 3: In the absence of ESC, the data for the ratio $C_O^{3pt}(t,\tau)/C^{2pt}(t)C^{2pt}(\tau-t)$ in the limits $(\tau-t) \to \infty$ and $t \to \infty$, should be independent of τ and t, i.e., the desired ground-state value given by a horizontal line about $t = \tau/2$. These examples of the current data [20] show large ESC. The gray band is the estimate of GSME given by a fit to the $n = 2$ truncated spectral function. In each column, the data are the same but the top panel shows a fit without the $N\pi$ state and the bottom with. The χ^2 of these two fits are similar.

4. Renormalization of lattice data

Results obtained with the lattice as the regulator, using a particular formulation of lattice QCD, and a particular choice of lattice operators need to be expressed in a scheme used by

phenomenologists, typically $\overline{MS}$ at scale $\mu = 2$ GeV. The renormalization of quark bilinears (calculation of the factors $Z_{A,S,T}$) is usually done non-perturbatively on the lattice at scale a using an intermediate scheme such as the regularization independent symmetric momentum subtraction (RI-sMOM) scheme [10, 11]. Results in this scheme are first matched to the continuum $\overline{MS}$ scheme at the same scale a (horizontal matching), and then run to the final scale, say $\mu = 2$ GeV. The last two steps in the calculation are done in the continuum using perturbation theory. Suffice to say this part of the calculation for nucleon charges is under control at the 1–2% level. See Appendix B in Ref. [20] for details.

5. Chiral-continuum-finite-volume extrapolation (CCFV)

The renormalized axial, $g_A^{u,d,s}$, and tensor, $g_T^{u,d,s}$, charges are extrapolated to the physical point, $a \to 0$, $M_\pi = 135$ MeV, and $M_\pi L \to \infty$, using the ansatz

$$g(a, M_\pi, M_\pi L) = c_0 + c_a a + c_2 M_\pi^2 + c_3 \frac{M_\pi^2 e^{-M_\pi L}}{\sqrt{M_\pi L}} . \tag{4}$$

It includes the leading corrections in the 3 variables $\{a, M_\pi, M_\pi L\}$. Note that the $O(a)$ term is pertinent to our lattice setup. It would be $c_a a^2$ if the action and operators were $O(a)$ improved. Also, higher order corrections are known but including them results in over parameterization with current data. Clearly, the goal is to increase the number of $\{a, M_\pi, M_K, M_\pi L\}$ points to be able to include higher order terms. In all calculations so far, there is no evidence for significant finite-volume corrections for $M_\pi L > 4$ [2]. So this correction is often dropped. Also, a term $\propto M_K^2$ is added to the analysis if it is not tuned to the physical value in the simulations.

The leading chiral contribution to $g_S^{u,d}$ is from a term $\propto M_\pi$, and the ansatz becomes [8]

$$g_S^{u,d}(a, M_\pi, M_\pi L) = d_0 + d_a a + d_2 M_\pi + d_3 M_\pi^2 + d_4 M_\pi \left(1 - \frac{2}{M_\pi L}\right) e^{-M_\pi L} . \tag{5}$$

Note that the finite-volume term is also modified. For the pion-nucleon sigma term, $\sigma_{\pi N} = m_l^{\rm bare} g_S^{u+d,{\rm bare}}$, the data are extrapolated using the N^{2}LO χPT expression [21]:

$$\sigma_{\pi N} = (d_2 + d_2^a a) M_\pi^2 + d_3 M_\pi^3 + d_4 M_\pi^4 + d_{4L} M_\pi^4 \log \frac{M_\pi^2}{M_N^2} . \tag{6}$$

Our χPT analysis [8] suggests all five terms contribute significantly. Typically, with data at only 3–4 values of M_π, one can effectively explore the chiral part of the ansatz with a maximum of three terms. One more term can be included by fixing the coefficient d_3^χ to its χPT value evaluated with $M_N = 0.939$GeV, $g_A = 1.276$, and $F_\pi = 92.3$MeV [8]. These CCFV extrapolations constitute a major uncertainty in current calculations. It is steadily decreasing as the number of $\{a, M_\pi, M_\pi L\}$ points, accumulated over a larger range in each variable, are simulated.

6. Status of results for $g^{u,d,s}_{A,S,T}$ and the σ-terms

The current status of the results for 2+1 and 2+1+1-flavor calculations that meet the FLAG criteria for averaging, is shown in Figs. 4 and 5 taken from Ref. [20]. Overall, all lattice data agree within 1σ. There are two notable ($\gtrsim 2\sigma$) differences: in g^u_A and $\sigma_{\pi N}$ between the most recent 2+1+1 flavor results from the PNDME [20] and the ETM [22] collaborations. These differences are mainly due to the handling of ESC, in particular of the $N\pi$ states. The PNDME analysis includes them, while in most cases the others, including ETM, do not or do not find evidence for them. This, again, highlights the already stated need to resolve the issue of the contribution of multihadron states in the analysis of ESC.

Note that, at the lowest order, the hadronic part of the interactions with dark matter or novel Higgs in an effective theory framework is $\overline{q}\Gamma q$, where Γ could be any element of the 16 Dirac gamma matrices. Thus, the full set of charges, $g^{u,d,s}_{A,P,S,T,V}$, provide the full set of couplings needed by phenomenologists and experimenters to describe these novel phenomena.

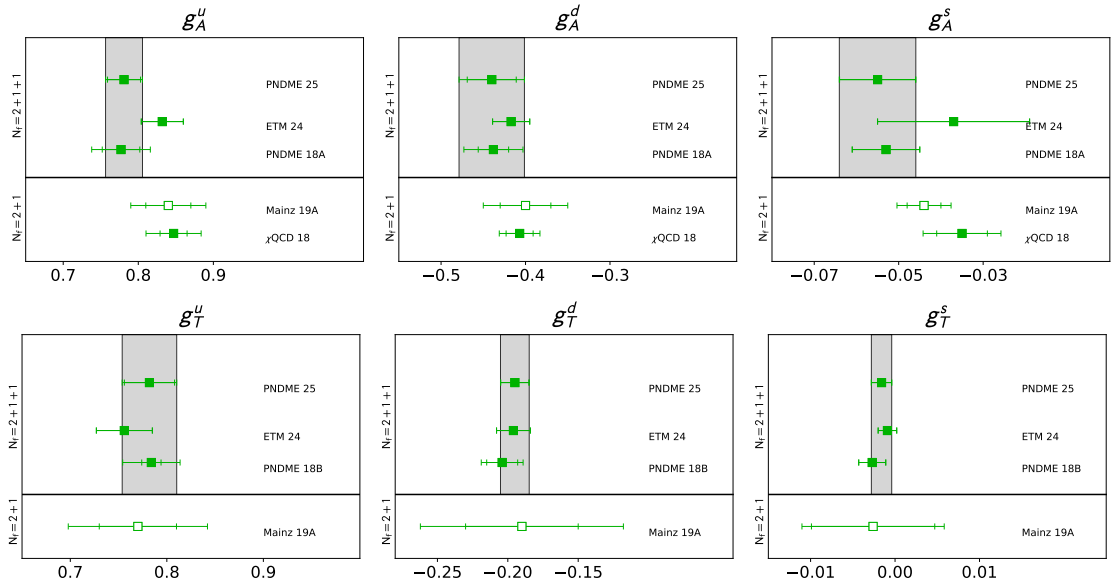

Figure 4: Comparison of lattice results obtained using 2+1+1 or 2+1-flavors of quarks that meet the FLAG criteria. Unfilled symbols indicate unpublished results or are conference proceedings. The references are PNDME 25 [20], ETM 24 [22] PNDME 18A [3] PNDME 18B [4] Mainz 19A [23] χQCD 18 [24].

7. The axial charges, $g^{u,d,s}_A$, and the nucleon spin

Phenomenologically, the key parameter quantifying the interactions of the neutron with the weak charged current is the isovector axial charge g^{u-d}_A. It is measured very accurately from the asymmetry parameter A (relative to the decay plane defined by the directions of the neutron spin and the emitted electron's direction) in the decay distribution of the neutron, $n \to p + e^- + \overline{\nu}_e$. High precision results for the ratio of the axial to the vector charge, g_A/g_V have been obtained in two experiments: (i) 1.2772(20) using polarized ultracold neutrons (UCN) by the UCNA collaboration [39, 40], and (ii) 1.27641(45)(33) using a cold neutron beam in PERKEO III [41, 42]. An open question is, given these precise measurements, can contributions expected

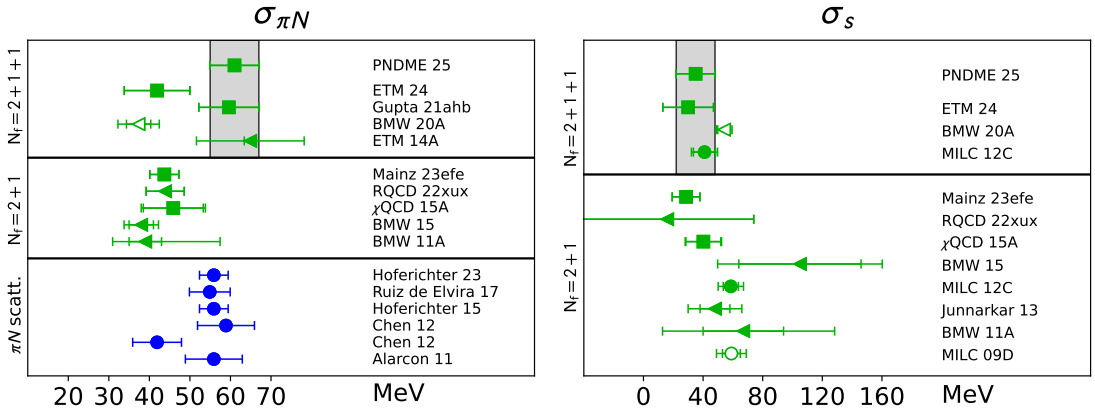

Figure 5: (Left) Results for $\sigma_{\pi N} = m_{ud} g_S^{u+d}$ from 2+1- and 2+1+1-flavor lattice calculations that satisfy the FLAG criteria for inclusion in averages. The BMW 20 1+1+1+1-flavor result is still a preprint and listed here under 2+1+1-flavor calculations for brevity. We follow the FLAG conventions and denote direct determinations by squares and the results obtained using the Feynman-Helmann method by triangles. The references for the lattice results are: PNDME 25 [20], ETM 24 [22], Gupta 21ahb [8], BMW 20A [25] ETM 14A [26], Mainz 23ehe [27] RQCD 22xux [28] χQCD 15A [29], BMW 15 [30], BMW 11A [25]. The phenomenological estimates (blue filled circles), obtained using πN scattering data, are from Hoferichter 23 [31], Ruiz de Elvira 17 [32], Hoferichter 15 [33], Chen 12 [34] Alarcon 11 [35]. (Right) Results for σ_s. The additional references for σ_s are MILC 12C [36], Junnarkar 13 [37], MILC 09D [38]

from BSM physics be resolved. For this an equally precise (to better than a part in a thousand) prediction of the value in QCD is needed [43, 44]. Reaching this precision is the goal of lattice QCD calculations but it is quite a way away—the FLAG 2024 report assigns an $\approx 2\%$ uncertainty to g_A^{u-d} [2]. For further discussion on g_A^{u-d}, see the talk by André Walker-Loud at this conference [45].

A gauge invariant decomposition of the nucleon's total spin into the sum of the contribution of (i) the intrinsic spin of the quark of flavor q, $\Delta q \equiv \Delta\Sigma_q \equiv \langle 1 \rangle_{\Delta q^+} \equiv g_A^q$; (ii) the orbital angular momentum of that quark, L_q; and (iii) the total angular momentum of the gluons J_g is given by Ji's sum rule [46]:

$$\frac{1}{2} = \sum_{q=u,d,s,c,.} \left(\frac{1}{2}\Delta q + L_q \right) + J_g \tag{7}$$

To explain the spin of the proton starting from QCD, all three terms needs to be calculated. The flavor diagonal charges give the first term, $\frac{1}{2}\Delta\Sigma \equiv \sum_{q=u,d,s} \frac{1}{2}\Delta q$. Our latest result, $\sum_{q=u,d,s} \frac{1}{2}\Delta q = 0.143(24)$ at 4 GeV^2 [20], is in good agreement with the COMPASS analysis $0.13 < \frac{1}{2}\Delta\Sigma < 0.18$ at 3 GeV^2 [47]. Note that, above 3 GeV^2 the change in the axial charges with scale is negligible.

8. Tensor charges, $g_T^{u,d,s}$, quark electric dipole moment, and transversity moment

I will use the electric dipole moment of the neutron (nEDM) to illustrate how BSM physics can give rise to novel phenomena at low energy and/or to provide corrections to the properties of hadrons. Most BSM models have new sources of $\not{C}\not{P}$. At low energies, a renormalization group analysis (integrating over momenta between the BSM scale Λ and the hadronic scale μ and integrating out heavy degrees of freedom) gives possible interactions (operators O composed of quarks and gluons)

organized by their dimension—the effective low-energy theory. One can determine their impact on low energy phenomena by calculating their ME between hadronic states using lattice QCD.

To motivate the connection between tensor charges and the quark EDM, consider the QCD Lagrangian in the presence of three $\not{C}\not{P}$ interactions—the Θ-term, which is allowed in the standard model, the quark EDM and the Weinberg three gluon operator, $\mathcal{W}$— at the hadronic scale μ (see Refs. [48, 49] for background)

$$\mathcal{L}_{\rm QCD} \longrightarrow \mathcal{L}^{\not{C}\not{P}}_{\rm QCD} = \mathcal{L}_{\rm QCD} - \frac{g^2}{32\pi^2}\Theta G_{\mu\nu}\tilde{G}_{\mu\nu} - i\frac{e}{2}\sum_q d_q\, \bar{q}\sigma^{\mu\nu}\tilde{F}_{\mu\nu}q + d_{\mathcal{W}}\, f^{abc}G^a_{\mu\nu}\tilde{G}^{\nu\beta,b}G^{\mu,c}_{\beta} \quad (8)$$

where $F_{\mu\nu}$ and $G_{\mu\nu}$ are the electromagnetic and chromo field strength tensors, $\tilde{G}^{\mu\nu} = \epsilon^{\mu\nu\alpha\beta}G_{\alpha\beta}/2$, and $\sigma_{\mu\nu} = (i/2)[\gamma_\mu, \gamma_\nu]$. The couplings, $d_q,\ d_{\mathcal{W}}$ are of the form c_i/Λ^{D-4} where c_i is the coupling at scale μ generated by a renormalization group analysis and D is the dimension of the operator. Note that the Θ-term is part of the SM, but is usually neglected under the assumption that some form of Peccei-Quinn mechanism relaxes $\Theta \to 0$ [50]. It, however, also gets contributions due to mixing with BSM operators, for example the Weinberg operator, under the renormalization group.

The electromagnetic properties of hadrons (nucleons in our case) are extracted from the ME of the electromagnetic current $J^{\rm EM}_\mu \equiv eV_\mu = e\sum_q \bar{q}\gamma_\mu q$ within the hadron ground state. Its Lorentz covariant parameterization in terms of the Dirac, F_1, Pauli, F_2, and electric dipole form factor, F_3, is

$$\langle N|J^{\rm EM}_\mu(q)|N\rangle = \overline{u}_N(p')\left[\gamma_\mu\ F_1(q^2) + i\frac{[\gamma_\mu,\gamma_\nu]}{2}q^\nu\ \frac{F_2(q^2)}{2M_N} - \frac{[\gamma_\mu,\gamma_\nu]}{2}q^\nu\gamma_5\ \frac{F_3(q^2)}{2M_N}\right]u_N(p), \quad (9)$$

where I have neglected the parity violating anapole form factor F_A. From these, the Sachs electric, $G_E = F_1 - (q^2/4M^2)F_2$, and magnetic form factors, $G_M = F_1 + F_2$, are obtained. Taking different momentum and spin projections of the real and imaginary parts of $\langle N|V_\mu(Q)|N\rangle$ give the charges (the electric charge is $G_E(0) = F_1(0) = 1$ due to CVC and the (anomalous) magnetic dipole moment is $F_2(0)/2M_N$). The form factor F_3 arises only if there are interactions that violate parity P and time reversal T invariances. Each $\not{C}\not{P}$ operator gives a contribution $F_3(0)/2M_N = d_n$ to the nEDM.

The change to the low energy physics (nEDM) on including $\not{C}\not{P}$ interactions can arise in two ways: a change in the probe (vector current) and through the presence of the new interactions in the Lagrangian. The Θ and Weinberg operators do not change the vector current. To get their contribution to the nEDM, one can use the small Θ and $d_{\mathcal{W}}$ approximation to expand the $\not{C}\not{P}$ part of $\mathcal{L}^{\not{C}\not{P}}_{\rm QCD}$ in the action e^{-S}. The leading order contribution is then given by the correlation of these operators with the vector current,

$$\langle\Omega|\mathcal{N}(\tau)V_\mu(t)\mathcal{N}(0)|\Omega\rangle\Big|^{\Theta}_{\not{C}\not{P}} = \left\langle \mathcal{N}(\tau)\left(V_\mu \int d^4x\ \Theta G^{\mu\nu}\tilde{G}^{\mu\nu}\right)(t)\ \mathcal{N}(0)\right\rangle, \quad (10)$$

$$\langle\Omega|\mathcal{N}(\tau)V_\mu(t)\mathcal{N}(0)|\Omega\rangle\Big|^{\mathcal{W}}_{\not{C}\not{P}} = \left\langle \mathcal{N}(\tau)\left(V_\mu \int d^4x\ d_{\mathcal{W}}\ f^{abc}G^a_{\mu\nu}\tilde{G}^{\nu\beta,b}G^{\mu,c}_{\beta}\right)(t)\ \mathcal{N}(0)\right\rangle. \quad (11)$$

In short, the presence of $\not{C}\not{P}$ operator changes the coupling of the vector current to the neutron by a tiny amount due to the generation of an EDM whose value is given by the correlation of the gluonic operator (Θ or $\mathcal{W}$) with the vector 3-point function. Parenthetically, the $\not{C}\not{P}$ modification $\overline{g}^0_S$ of

the pion-nucleon coupling $g_{\pi NN}$ is obtained by a similar calculation with V_μ replaced by the axial current A_μ in Eqs. (10) and (11).

The leading contribution of the quark EDM operator to nEDM comes from a new term, $\frac{i}{2}\sum_q d_q\ \overline{q}\sigma^{\mu\nu}q$, in the vector current derived from the $\mathcal{L}^{\not{C}\not{P}}_{QCD}$ using the Noether's theorem. Its ME are the tensor charges $g_T^{u,d,s}$ and their contribution to the nEDM is $\sum_q d_q g_T^q$. These charges, in particular $g_T^{u,d}$, are well determined, while g_T^s is tiny, however reducing the uncertainty in it is important if d_s is enhanced by m_s as expected if the BSM $\not{C}\not{P}$ interactions are Higgs-like. An analysis of the constraints on the $\not{C}\not{P}$ couplings d_q using our lattice QCD values for $g_T^{u,d,s}$ has been presented in Refs. [4], and these d_q in the split SUSY scenario with gaugino mass unification [51–53]. So far, in lattice QCD calculations of the contribution of various operators to nEDM, the charges $g_T^{u,d,s}$ giving the contribution of the quark EDM operators, are the only robust numbers.

Results for the contribution of the Θ-term to nEDM (after the understanding of, and taking into account, the phase $e^{i\Theta\alpha_5^O\gamma_5}$ that arises in the nucleon spinor due to each $\not{C}\not{P}$ operator O in Ref. [54]) have been presented in Refs. [55–58]. At first sight, in terms of collecting lattice data, this is a controlled calculation requiring weighting the matrix element of the vector current by the topological charge Q on each lattice. Getting a statistical signal in $F_3(0)$ and the systematics have, however, proven to be challenging. Practitioners have used various methods to calculate Q: the integral $\int d^4x\ G^{\mu\nu}\tilde{G}^{\mu\nu}$ using gauge links on gradient flowed lattices [55, 57], the fermion method using the pseudoscalar density [56], and the overlap Dirac operator [58]. These give similar results. For renormalization, one basically needs only Z_V, which is well determined.

Overall, the validity of these results lies in the practitioner's eye! In Refs. [55, 58], the calculations were done on ensembles with $M_\pi > 339$ MeV and the data extrapolated to the physical $M_\pi = 135$ MeV. The fit and the error at $M_\pi = 135$ MeV is dominated by the use of the constraint $d_n/\Theta = 0$ at $M_\pi = 0$. In my opinion, more data closer to $M_\pi = 135$ MeV are needed to validate both the chiral fit and the value.

The Los Alamos group [57] do have data at $M_\pi \approx 135$ MeV, which by itself, and consequently the final result, has much larger errors. The more important issue they raise is whether $N\pi$ states should be included in removing ESC as suggested by a χPT analysis. Unfortunately, the result even changes sign between the two analyses. My overall conclusion is much more work needs to be done to get data closer to $M_\pi = 135$ MeV, increase statistical precision and resolve the ESC conundrum.

The lattice calculations of the remaining leading $\not{C}\not{P}$ operators: the quark chromo EDM [59], the Weinberg [60] and the 4-fermion operators are in even earlier stages of development.

9. Scalar charges $g_S^{u,d,s}$, the pion-nucleon sigma term $\sigma_{N\pi}$, the strangeness content σ_s

The matrix elements of the flavor diagonal scalar quark bilinear operators are used to calculate the pion-nucleon sigma term $\sigma_{N\pi}$, which gives the dependence of the nucleon mass on the quark mass, and the strangeness content y of the nucleon. These are defined as

$$\sigma_{\pi N} = m_l\langle N|\bar{u}u + \bar{d}d|N\rangle = m_l\frac{\partial M_N}{\partial m_l}\,, \qquad \sigma_s = m_s\langle N|\bar{s}s|N\rangle\,, \qquad y = \frac{2\langle N|\bar{s}s|N\rangle}{\langle N|\bar{u}u + \bar{d}d|N\rangle}\,. \quad (12)$$

Two methods have been used to calculate these ME: (i) the direct evaluation of the matrix elements (sum of the connected and disconnected contributions from the quark line diagrams shown in Fig. 1),

and (ii) using the Feynman-Hellmann theorem to evaluate the derivative of the nucleon mass with respect to the quark mass. The equality of the two methods for $\sigma_{\pi N}$ is shown in Eq. (12). The world data for $\sigma_{\pi N}$ and σ_s is shown in Fig. 5 using the FLAG format.

The average of lattice QCD results from 2+1-flavor simulations given in the FLAG 2024 report, which predates the results in [20] is $\sigma_{\pi N}|_{\text{no N}\pi} = 42.2(2.4)$ MeV [2], while the latest phenomenological analysis using the $N\pi$ scattering data, and including corrections due to isospin violations [31], is $\sigma_{\pi N}|_{\text{pheno}} = 55.9(3.6)$ MeV. On the other hand, our lattice QCD result including the $N\pi$ state in the analysis gave $\sigma_{\pi N}|_{N\pi} = 59.6(7.4)$ MeV and without it $\sigma_{\pi N}|_{\text{no N}\pi} = 41.9(4.9)$ MeV [8] (updated to $\sigma_{\pi N}|_{N\pi} = 61(6)$ MeV and $\sigma_{\pi N}|_{\text{no N}\pi} = 42(6)$ MeV in [20]). Thus, the main issue confronting lattice calculations is—should the $N\pi$ state be included in the analysis? If yes, as suggested by χPT [8], then our $\sigma_{\pi N}|_{N\pi}$ suggests no tension between the lattice QCD and the phenomenological result, otherwise there is an $\approx 4.5\sigma$ tension. Hopefully, more precise lattice calculations underway will shed light on this issue. For dark matter direct detection experiments, a larger $g_S^{u,d}$ is good news since the cross-section in the favored scalar channel is $\propto (g_S^{u,d})^2$.

In the case of σ_s, the lightest multihadron intermediate state in Fig. 1 (middle) would be ΣK, which is heavier than $N(1440)$. Thus the standard analyses is appropriate. The FLAG 2024 report gives $\sigma_s = 41.0(8.8)$ MeV (44.9(6.4) MeV) for the 2+1+1-flavor (2+1-flavor) theory. Our 2+1+1-flavor result, $\sigma_s|_{\text{no N}\pi} = 35(13)$ MeV [20], is consistent but has much larger uncertainty as shown in Fig. 5.

10. Conclusions and Future Prospects

Lattice QCD results for all the charges will, steadily over time, continue to improve in precision. The slowest part of the numerical calculation is of the disconnected diagrams and new ideas would help. The two largest systematics in current results are removing the contributions of excited states and the CCFV extrapolation to get physical results. The second can be addressed by increasing the number and range of $\{a, M_\pi, M_\pi L\}$ points simulated close to the physical pion mass, and increasing the statistics. The community is doing this. I see accelerating the calculation of the disconnected contributions and removing the contribution of excited states as the main bottlenecks. Of course, underlying it all is the S2N problem due to the exponential, $e^{M_N - 1.5M_\pi}$, growth of the noise in all n-point nucleon correlation functions. Is this an inherent problem or waiting for a clever idea?

My estimate is the community will reach an overall 1% precision in all isovector charges in the next five years. For the flavor-diagonal charges, $g_{A,T}^{u,d}$, results with 2% precision should be attainable. The main limiting factor will be the amount of resources devoted to the calculations of the disconnected diagrams. The charges $g_{A,T}^{s}$ are small in magnitude and a 20% precision would be a good target.

The most interesting case is of the scalar charges $g_S^{u,d,s}$. Resolving whether multihadron $N\pi$ states make significant contributions to the respective correlation functions is the key bottleneck. Numerical tools and algorithms developed to first reduce their contribution in the correlation functions simulated coupled with data-driven analysis strategies to remove the remaining contributions using their spectral decomposition will have a broad impact on the field.

Acknowledgments

For the calculations by the Los Alamos centered collaborations, I thank the MILC collaboration for providing the HISQ ensembles. Many thanks to Sungwoo Park who carried out most of the analysis presented here and to my long-term collaborators Tanmoy Bhattacharya, Vincenzo Cirigliano and Emanuelle Mereghetti from whom I learned much. These calculations used the Chroma software suite [61] and resources at (i) the National Energy Research Scientific Computing Center, a DOE Office of Science User Facility supported by the Office of Science of the U.S. Department of Energy under Contract No. DE-AC02-05CH11231; (ii) the Oak Ridge Leadership Computing Facility, which is a DOE Office of Science User Facility supported under Contract DE-AC05-00OR22725, through awards under the ALCC program projects LGT107 and hep145; and an INCITE award HEP133; (iii) the USQCD collaboration, which is funded by the Office of Science of the U.S. Department of Energy; and (iv) Institutional Computing at Los Alamos National Laboratory. R.G. was partly supported by the U.S. Department of Energy, Office of Science, Office of High Energy Physics under Contract No. DE-AC52-06NA25396, and partly by the LANL LDRD program.

References

[1] Flavour Lattice Averaging Group (FLAG) collaboration, Y. Aoki et al., *Eur. Phys. J. C* **82** (2022) 869 [2111.09849].
[2] Flavour Lattice Averaging Group (FLAG) collaboration, Y. Aoki et al., 2411.04268.
[3] H.-W. Lin, R. Gupta, B. Yoon, Y.-C. Jang and T. Bhattacharya, *Phys. Rev.* **D98** (2018) 094512 [1806.10604].
[4] R. Gupta, B. Yoon, T. Bhattacharya, V. Cirigliano, Y.-C. Jang and H.-W. Lin, *Phys. Rev.* **D98** (2018) 091501 [1808.07597].
[5] R. Gupta, *Universe* **10** (2024) 135 [2401.16614].
[6] T. Bhattacharya, V. Cirigliano, S. D. Cohen, A. Filipuzzi, M. Gonzalez-Alonso, M. L. Graesser et al., *Phys. Rev. D* **85** (2012) 054512 [1110.6448].
[7] R. Gupta, Y.-C. Jang, B. Yoon, H.-W. Lin, V. Cirigliano and T. Bhattacharya, *Phys. Rev.* **D98** (2018) 034503 [1806.09006].
[8] R. Gupta, S. Park, M. Hoferichter, E. Mereghetti, B. Yoon and T. Bhattacharya, *Phys. Rev. Lett.* **127** (2021) 242002 [2105.12095].
[9] R. Babich, J. Brannick, R. C. Brower, M. A. Clark, T. A. Manteuffel, S. F. McCormick et al., *Phys. Rev. Lett.* **105** (2010) 201602 [1005.3043].
[10] G. Martinelli, C. Pittori, C. T. Sachrajda, M. Testa and A. Vladikas, *Nucl. Phys. B* **445** (1995) 81 [hep-lat/9411010].
[11] C. Sturm, Y. Aoki, N. H. Christ, T. Izubuchi, C. T. C. Sachrajda and A. Soni, *Phys. Rev.* **D80** (2009) 014501 [0901.2599].
[12] G. Parisi, *Phys. Rept.* **103** (1984) 203.
[13] G. P. Lepage, in *Boulder ASI 1989:97-120*, pp. 97–120, 1989, http://alice.cern.ch/format/showfull?sysnb=0117836.

[14] Y.-C. Jang, R. Gupta, B. Yoon and T. Bhattacharya, *Phys. Rev. Lett.* **124** (2020) 072002 [1905.06470].
[15] Nucleon Matrix Elements (NME) collaboration, S. Park, R. Gupta, B. Yoon, S. Mondal, T. Bhattacharya, Y.-C. Jang et al., *Phys. Rev. D* **105** (2022) 054505 [2103.05599].
[16] Precision Neutron Decay Matrix Elements (PNDME) collaboration, Y.-C. Jang, R. Gupta, T. Bhattacharya, B. Yoon and H.-W. Lin, *Phys. Rev. D* **109** (2024) 014503 [2305.11330].
[17] Y.-C. Jang, R. Gupta, H.-W. Lin, B. Yoon and T. Bhattacharya, *Phys. Rev. D* **101** (2020) 014507 [1906.07217].
[18] RQCD collaboration, G. S. Bali, L. Barca, S. Collins, M. Gruber, M. Löffler, A. Schäfer et al., *JHEP* **05** (2020) 126 [1911.13150].
[19] L. Barca, G. Bali and S. Collins, *Phys. Rev. D* **107** (2023) L051505 [2211.12278].
[20] S. Park, R. Gupta, T. Bhattacharya, F. He, S. Mondal, H.-W. Lin et al., 2503.07100.
[21] M. Hoferichter, J. Ruiz de Elvira, B. Kubis and U.-G. Meißner, *Phys. Rept.* **625** (2016) 1 [1510.06039].
[22] C. Alexandrou, S. Bacchio, J. Finkenrath, C. Iona, G. Koutsou, Y. Li et al., *Phys. Rev. D* **111** (2025) 054505 [2412.01535].
[23] D. Djukanovic, H. Meyer, K. Ottnad, G. von Hippel, J. Wilhelm and H. Wittig, *PoS* **LATTICE2019** (2019) 158 [1911.01177].
[24] [χQCD 18] J. Liang, Y.-B. Yang, T. Draper, M. Gong and K.-F. Liu, *Phys. Rev.* **D98** (2018) 074505 [1806.08366].
[25] S. Borsanyi, Z. Fodor, C. Hoelbling, L. Lellouch, K. K. Szabo, C. Torrero et al., 2007.03319.
[26] C. Alexandrou, V. Drach, K. Jansen, C. Kallidonis and G. Koutsou, *Phys. Rev. D* **90** (2014) 074501 [1406.4310].
[27] A. Agadjanov, D. Djukanovic, G. von Hippel, H. B. Meyer, K. Ottnad and H. Wittig, *Phys. Rev. Lett.* **131** (2023) 261902 [2303.08741].
[28] RQCD collaboration, G. S. Bali, S. Collins, P. Georg, D. Jenkins, P. Korcyl, A. Schäfer et al., *JHEP* **05** (2023) 035 [2211.03744].
[29] xQCD collaboration, Y.-B. Yang, A. Alexandru, T. Draper, J. Liang and K.-F. Liu, *Phys. Rev. D* **94** (2016) 054503 [1511.09089].
[30] S. Durr et al., *Phys. Rev. Lett.* **116** (2016) 172001 [1510.08013].
[31] M. Hoferichter, J. R. de Elvira, B. Kubis and U.-G. Meißner, *Phys. Lett. B* **843** (2023) 138001 [2305.07045].
[32] J. Ruiz de Elvira, M. Hoferichter, B. Kubis and U.-G. Meißner, *J. Phys. G* **45** (2018) 024001 [1706.01465].
[33] M. Hoferichter, J. Ruiz de Elvira, B. Kubis and U.-G. Meißner, *Phys. Rev. Lett.* **115** (2015) 092301 [1506.04142].
[34] Y.-H. Chen, D.-L. Yao and H. Q. Zheng, *Phys. Rev. D* **87** (2013) 054019 [1212.1893].
[35] J. M. Alarcon, J. Martin Camalich and J. A. Oller, *Phys. Rev. D* **85** (2012) 051503 [1110.3797].
[36] C. McNeile, A. Bazavov, C. T. H. Davies, R. J. Dowdall, K. Hornbostel, G. P. Lepage et al., *Phys. Rev. D* **87** (2013) 034503 [1211.6577].

[37] P. Junnarkar and A. Walker-Loud, *Phys. Rev. D* **87** (2013) 114510 [1301.1114].
[38] MILC collaboration, D. Toussaint and W. Freeman, *Phys. Rev. Lett.* **103** (2009) 122002 [0905.2432].
[39] UCNA Collaboration, M. Mendenhall et al., *Phys.Rev.* **C87** (2013) 032501 [1210.7048].
[40] UCNA collaboration, M. A. P. Brown et al., *Phys. Rev.* **C97** (2018) 035505 [1712.00884].
[41] B. Märkisch et al., *Phys. Rev. Lett.* **122** (2019) 242501 [1812.04666].
[42] D. Mund, B. Maerkisch, M. Deissenroth, J. Krempel, M. Schumann, H. Abele et al., *Phys. Rev. Lett.* **110** (2013) 172502 [1204.0013].
[43] R. Alarcon et al., 2308.09059.
[44] S. Alioli, V. Cirigliano, W. Dekens, J. de Vries and E. Mereghetti, *JHEP* **05** (2017) 086 [1703.04751].
[45] Z. B. Hall et al., 2503.09891.
[46] X.-D. Ji, *Phys. Rev. Lett.* **78** (1997) 610 [hep-ph/9603249].
[47] COMPASS collaboration, C. Adolph et al., *Phys. Lett. B* **753** (2016) 18 [1503.08935].
[48] M. Pospelov and A. Ritz, *Annals Phys.* **318** (2005) 119 [hep-ph/0504231].
[49] J. Engel, M. J. Ramsey-Musolf and U. van Kolck, *Prog. Part. Nucl. Phys.* **71** (2013) 21 [1303.2371].
[50] R. D. Peccei and H. R. Quinn, *Phys. Rev. Lett.* **38** (1977) 1440.
[51] N. Arkani-Hamed and S. Dimopoulos, *JHEP* **06** (2005) 073 [hep-th/0405159].
[52] G. F. Giudice and A. Romanino, *Nucl. Phys. B* **699** (2004) 65 [hep-ph/0406088].
[53] N. Arkani-Hamed, S. Dimopoulos, G. F. Giudice and A. Romanino, *Nucl. Phys. B* **709** (2005) 3 [hep-ph/0409232].
[54] M. Abramczyk, S. Aoki, T. Blum, T. Izubuchi, H. Ohki and S. Syritsyn, *Phys. Rev. D* **96** (2017) 014501 [1701.07792].
[55] J. Dragos, T. Luu, A. Shindler, J. de Vries and A. Yousif, *Phys. Rev. C* **103** (2021) 015202 [1902.03254].
[56] C. Alexandrou, A. Athenodorou, K. Hadjiyiannakou and A. Todaro, *Phys. Rev. D* **103** (2021) 054501 [2011.01084].
[57] T. Bhattacharya, V. Cirigliano, R. Gupta, E. Mereghetti and B. Yoon, *Phys. Rev. D* **103** (2021) 114507 [2101.07230].
[58] χQCD collaboration, J. Liang, A. Alexandru, T. Draper, K.-F. Liu, B. Wang, G. Wang et al., *Phys. Rev. D* **108** (2023) 094512 [2301.04331].
[59] T. Bhattacharya, V. Cirigliano, R. Gupta, E. Mereghetti, J.-S. Yoo and B. Yoon, *Phys. Rev. D* **108** (2023) 074507 [2304.09929].
[60] T. Bhattacharya, S. Bhattacharya, V. Cirigliano, R. Gupta, E. Mereghetti, S. Park et al., *PoS* **LATTICE2024** (2025) 344 [2502.00460].
[61] SciDAC Collaboration, LHPC Collaboration, UKQCD Collaboration, R. G. Edwards and B. Joo, *Nucl. Phys. Proc. Suppl.* **B140** (2005) 832 [hep-lat/0409003].

PoS(QCHSC24)009